Pakistan Journal of Science, 71 (4 Suppl.): 2019, Page 222-229
ISSN: 2411-0930

MULTIQUADRIC RADIAL BASIS APPROXIMATION FOR SPECKLE NOISE REMOVAL

M.A. Khan[1,*], H. Khan[1], S. Khan[1], Z.H. Khan[2], K. Khattak[2], S. Khan[1], J. Khan[1], M. Ali[1] and N. Iqbal[1]

[1]University of Engineering and Technology Mardan, Khyber Pakhtunkhwa, Pakistan
[2]University of Engineering and Technology Peshawar, Khyber Pakhtunkhwa, Pakistan
*Corresponding author's E-mail: mushtaq@uetmardan.edu.pk

ABSTRACT: In this article a new meshless scheme to address image restoration having speckle noise is proposed. This scheme combines the Total Variation norm (TV) with Radial Basis Function (RBF) approximation to solve the associated Partial Differential equation (PDF) with the minimization functional model for the smooth solution and to get the good denoising result. This algorithm of meshless is based on local collocation along with Multiquadric Radial Basis Function (MQ-RBF). The experimental results demonstrate that our proposed meshless scheme regarding image denoising and improved peak-signal- to- noise ratio in comparison to traditional TV-based method.

Keywords: Image restoration; Total variation (TV) regularization; Radial basis functions (RBFs).

INTRODUCTION

Denoising of the image is an important task in various applications in both image processing and mathematics. Multiplicative noise is one of the challenging issues in nowadays science and engineering. Speckle noise is likewise a kind of multiplicative clamor that shows up in various real and artificial images. In this work, we will consider on image restoration having speckle noise. Multiplicative /speckle noise is modeled as:

$$f = g.\eta_1, \qquad (1)$$

where f is the degrade picture having multiplicative (speckle) noise η_1 and g is the clean picture. In literature, many useful models have been used to tickle this problem, but variational models based on (TV) norm have achieved great success in image restoration, see (Shi *et al.*, 2008; Zhao *et al.*, 2014). In this direction, various traditional mesh-based schemes have been used by the researchers to solve the TV-based models having multiplicative (speckle) noise and to get the good restoration results, for more information (Shi *et al.*, 2008; Zhao *et al.*, 2014).But there is space for improvement.

Radial basis function (RBF) schemes have become more popular due to its meshless applications in science and engineering in past few decades approximation approach is certainly meshless and is primarily based on collocation in a fixed of scattered nodes for obtaining smooth data (Chen *et al.*, 2014). For further information of RBF collocation methods, see (Chen *et al.*, 2016; Singh and Kumar, 2017; Vertnik and Šarler, 2013; Sajavicius 2013; Jankowsa *et al.*, 2018). The most common and widely used RBF scheme for the letter class problems is the RBF collocation method, which is also known as Kansa method. The importance of this collocation method due to its meshless applications which means that only a set of points is required in the discretization of the continuous problem which leads the system into the nonlinear system of equations. This application of this method shows that this method is very easy to implement, problem in complex shape or in two and three dimensions and hence superior to the traditional scheme. This method is also called the RBF collocation method (RBFCM). RBF approximation approach is certainly meshless and is primarily based on collocation in a fixed of scattered nodes for obtaining smooth data (Dehghan *et al.*, 2015).

MATERIALS AND METHODS

The TV norm is one of the important tool for image restoration and numerical. For a given picture $g:\Omega \to R^2$, the TV regularization is given as under.

$$TV(g) = \int_\Omega |\nabla g| dxdy, \qquad (2)$$

where, $|\nabla g| = \sqrt{g_x^2 + g_y^2}$. The minimization functional of RLO model for model equation (1) is defined as under.

$$\min_g \left\{ J(g)dxdy + \alpha_1 \int_\Omega \frac{f}{g} dxdy + \alpha_2 \int_\Omega \left(\frac{f}{g} - 1 \right)^2 dxdy \right\}, (3)$$

$$J(g)=\int_{\Omega}|\nabla g|dxdy$$

where . In equation (3) the first part in TV functional is known as regularized term which is responsible for edge preservation, while the next two parts are known data fidelity terms, where α_1 and α_2 are called the parameters and are used for image de-noising. The minimization functional (2) leads to the flowing time marching Euler-Lagrange equation.

$$\frac{dg}{dt}=\nabla.\frac{\nabla g}{|\nabla g|}+\alpha_1\frac{f^2}{g^3}+\alpha_2\frac{f}{g^2}$$

Radial basis function approximation: Let us describe the RBF method now (Khan *et al.*,, 2017). For an Euclidean space R^d be d-dimensional, $\phi: R^d \to R$ be an invariant function at a pixel $x \in R^d$, then for $s \in R^d$, fixed point (center) s, the RBF is written as $\phi\left(\|x-s\|\right)$, where ϕ is known as RBF. The value $r=\|x-s\|$ is selected as Euclidean norm. Inverse Multiquadric (IMQ), Multiquadric (MQ) and Gaussian (GA) are some normally used RBFs having shape parameters which are a useful factor in RBF approximation.

Let $f(x), x \in \Omega \subset R^n$ be a multivariate function $\{y_j\}_{j=1}^{N}$ be the N interpolation function values, where Ω is bounded domain. For the data location points (centers) $\{x_i\}_{i=1}^{N} \in \Omega \subset R^n,$ then by RBF approximation $f(x)$ is approximated as;

$$S(x)=\sum_{j=1}^{N}\beta_j\varphi(\| x-x_j \|_2), \quad x \in \Omega, \quad (5)$$

in which β_j is the undefined coefficient and will be determined. By collocation method the above equation (5) can be rewritten as (Khan *et al.*,, 2017; Singh et al., 2017; Li et al.,2007).

$$w_i=S(x_i)=\sum_{j=0}^{N}\beta_j\phi(\| x_i-x_j \|_2), 1 \le i, j \le N. \quad (5)$$

Equation (5) results in the following NxN matrix linear system: $C\beta=e,$ in which $\beta=\left(\beta_1,\beta_{2,}.....,\beta_n\right)^T$ and will be determined and $e=(w_1,w_2,.....,w_n)^T$. The interpolation matrix of the RBF is defined as

$$C=[\phi_{ij}]=[\varphi(\| x_i-x_j \|_2)], \text{ for } 1 \le i, j \le N \text{ and } \phi_{ij}=\phi_{ji}. \quad (6)$$

In the above system C is NxN matrix, β and e are $Nx1$ matrices. The invariability of the above system is discussed. Equation (5) without polynomial term is formulated as under.

$$S(x)=\sum_{j=1}^{N}\beta_j\phi(\| x-x_j \|_2)+\sum_{i=1}^{M}\beta_{N+1}L_i(x), (7)$$

Constraints

$$\sum_{i=1}^{M}\beta_j L_i(x_j)=0, \quad 1 \le i \le M, \quad (8)$$

where $L_i \in \Pi_{n-1}$,$1 \le i \le M,$ while Π_n represents the total degree of all polynomials n in N variables, $\binom{N+n-1}{n-1}$.

The interpolation of (7) and (8) results in matrix system of equations of order $(M+N)X(M+N)$ which is given as under.

$$\begin{bmatrix} C & L \\ L^t & O \end{bmatrix}\begin{bmatrix} \beta \\ 0 \end{bmatrix}=\begin{bmatrix} a \\ 0 \end{bmatrix}. \quad (9)$$

where

$C_{i,j}=[\phi_{ij}]=[\varphi(\| x_i-x_j \|_2)], \ 1 \le i, j \le N$ indicates the entries of C, $L_{i,j}=L_i[x_j]$ with $1 \le i \le N$ and $1 \le j \le M,$ and O are $M \times N$ matrix. For more details regarding the RBFs with positive definiteness (PD), RBFs with shape parameter $c,$ and RBFs conditionality positive definiteness (CPD).

Gradient Projection Scheme (GP): The numerical approximation for (4) is defined as:

$$\frac{g^{(n+1)}-g^{(n)}}{dt}=\frac{\partial}{\partial x}\left(\frac{g_x^{(n)}}{\sqrt{(g_x^2)^{(n)}+(g_y^2)^{(n)}}}\right)+\frac{\partial}{\partial y}\left(\frac{g_x^{(n)}}{\sqrt{(g_x^2)^{(n)}+(g_y^2)^{(n)}}}\right)+\alpha_1\frac{(f)^0}{\left(g^3\right)^n}+\alpha_2\frac{(f)^0}{\left(g^2\right)^n},$$

or

$$g^{n+1} = g^n + dt\left[\begin{array}{l} \dfrac{g_{xx}^n}{\left(\sqrt{g_x^2}\right)^n + \left(\sqrt{g_y^2}\right)^n} + \\ \dfrac{g_{yy}^n}{\left(\sqrt{g_x^2}\right)^n + \left(\sqrt{g_y^2}\right)^n} + \\ \alpha_1 \dfrac{(f)^0}{\left(g^3\right)^n} + \alpha_2 \dfrac{(f)^0}{\left(g^2\right)^n} \end{array}\right] \quad (10)$$

Proposed Meshless Scheme (MS): In this subsection we introduce a novel meshless scheme by combining the TV norm along with MQ-RBF for the numerical solution of (3) for clean image g. The resultant Euler-Lagrange equation in this case is given as follow:

$$\frac{dg}{dt} = \frac{\left(g_{xx}+g_{yy}\right)\left(g_x^2+g_y^2\right) - \left(2g_x g_y g_{xy} + g_x^2 g_{xx} + g_y^2 g_{yy}\right)}{\left(g_x^2+g_y^2\right)^{\frac{1}{2}}}$$

$$+\alpha_1 \frac{f^2}{g^3} + \alpha_2 \frac{f}{g^2} \quad (11)$$

Suppose $\{x_i\}_{i=1}^N$ is the N different assessment data points in $\Omega \subseteq \Re^2$, where Ω represents a close domain [30]. Hence for each RBF, the subsequent equation is fulfilled, $\varphi(r) = \|r\|_2$ in $\Re^2$ and $r = (x, y)$. Given $\{xc_j\}_{j=1}^{Nc}$ Nc data center points, then RBF condition with no polynomial term added is written as under.

$$S(x) = \sum_{j=1}^{Nc} \beta_j \varphi(\| x - xc_j \|_2), \quad (12)$$

where β_j are the unknown coefficients in the RBF condition. The following interpolation condition is utilized to find the values of β_j

$$S(x_j) = f. \quad (13)$$

Equation (7) generates a nonlinear system of equations of order $Nc \times Nc$ and is written as:

$$D\beta = f, \quad (14)$$

which is used to find the expansion coefficients of β, where $\beta = (\beta_1, \beta_2, \ldots\ldots\ldots \beta_{Nc})^T$ and $f = (f_1, f_2, \ldots\ldots\ldots f_{Nc})^T$ are $Nc \times 1$ matrices, while matrix D shows system matrix, and is written as:

$$D = [\phi_{ij}] = [\varphi(\| xc_i - xc_j \|_2)],\ \mathrm{I} \le i, j \le N.$$

Matrix D is $Nc \times Nc$ order system matrix and is continually nonsingular because of its positive definiteness nature. Thus we have

$$\beta = D^{-1} f, \quad (15)$$

The interpolation condition (12) is utilizing on N assessment data points $\left(\{x_i\}_{j=1}^N\right)$ and hence $(NxNc)$ evaluation matrix E is obtained.

$$E = [\phi_{ij}] = [\varphi(\| x_i - xc_j \|_2)],\ {}_{1 \le i, j \le N, Nc}.$$

To evaluate the value of g at N data points, the following matrix vector product is used.

$$g = E\beta. \quad (16)$$

Combining equations (15) and (16) the following equation is obtained.

$$g = ED^{-1} f,\ g = Ff \quad (17),$$

where $F = ED^{-1}$, which is $Nx1$ matrix and indicated the approximate solution at any point in Ω. From equations (11) and (17) a new PDE is obtained, which given by the given nonlinear equation.

$$\frac{g^{n+1} - g^n}{dt} = \left[\begin{array}{l} \dfrac{\left(g_{xx}^n + g_{yy}^n\right)\left(\left(g_x^2\right)^n + \left(g_y^2\right)^n\right)}{\left(\left(g_x^2\right)^2 + \left(g_y^2\right)^2\right)^{\frac{1}{2}}} + \\ -\dfrac{\left(\begin{array}{l} 2g_x^n g_y^n \left(g_x g_y^n + g_y g_x^n\right) + \\ \left(g_x^2\right)^n g_{xx}^n + \left(g_y^2\right)^2 g_{yy}^n \end{array}\right)}{\left(\left(g_x^2\right)^2 + \left(g_y^2\right)^2\right)^{\frac{1}{2}}} + \\ \alpha_1 \dfrac{\left(f^2\right)^0}{\left(g^3\right)^n} + \alpha_2 \dfrac{f^0}{\left(g^2\right)^n} \end{array}\right],$$

$$M\left(g^n\right) g^{n+1} = M\left(g^n\right) g^n +$$

$$dt\left[\begin{array}{l} \left(g_{xx}^n + g_{yy}^n\right)\left(\left(g_x^2\right)^n + \left(g_y^2\right)^n\right) \\ -\left(\begin{array}{l} 2g_x^n g_y^n \left(g_x g_y^n + g_y g_x^n\right) + \\ \left(g_x^2\right)^n g_{xx}^n + \left(g_y^2\right)^2 g_{yy}^n \end{array}\right) \end{array}\right] +$$

$$dtM\left(g^n\right)\left[\alpha_1 \frac{\left(f^2\right)^0}{\left(g^3\right)^n} + \alpha_2 \frac{f^0}{\left(g^2\right)^n}\right], \quad (18)$$

$M(g)=\left(g_x^2+g_y^2\right)^{\frac{3}{2}}$, $g_x=F_x f$, $g_y=F_y f$, $g_{xx}=F_{xx} f$, $g_{yy}=F_{yy} f$, and $f^0=0$.

As RBF collocation scheme is not required to satisfy the restoration PDE (18), so we have the freedom to select any RBF. Multiquadric (MQ) a recognized RBF in Kansa scheme (Chen *et al.*, 2014) which reflects best results if an appropriate value of shape parameter c is chosen. All the parameters, i.e., the shape parameter c and regularization parameters α_1 and α_2 used in proposed meshless scheme MS depend upon the level of noise in image and the size of image and play a vital role in image resonation and are selected by the "Head and Trail" rule. The derivatives of the proposed scheme are same as done in (Khan *et al.*,, 2017).

RESULTS AND DISCUSSION

This section is dedicated to reveal the efficiency of the new meshless scheme MS. To compare the results of the two schemes GP and MS, we apply the two schemes on several artificial and real images for image restoration performance. The various selected images for experimental analysis are "Butterfly", "Peppers", "SynImage1", and "SynImage2", which are shown in Fig. 1. Speckle noise (with mean value 0 and variance L) is chosen as test noise in this study. For our meshless scheme MS, we choose $N=N_c$ is which is the same as the selected image size to check the image restoration results and to compare them with the mesh-based scheme GP. To evaluate the quality of the restored image, the peak signal-to-noise ratio (PSNR) is considered. PSNR is calculated by the given formula (Jiang *et al.*, 2015; Ullah *et al.*, 2016).

$$PSNR = 10 * log_{10}\left[\frac{M \times Nmax\{\hat{z}\}^2}{\| \hat{z} - z \|^2}\right]$$

$$\left[\frac{M \times Nmax\{g\}}{\left\| \equiv{g} - g \right\|^2}\right], \qquad (19)$$

where g indicates the original picture, and $\equiv{g}$ represents the resultant denoised picture while MxN shows the size of the selected image. The new meshless scheme MS will be stopped regarding iterations by the given formula.

$$\frac{\| u^{(k+1)} - u^{(k)} \|}{\| u^{(k)} \|} \leq \text{ò}, \qquad (20)$$

with ε express the maximal acceptable error. In this study, we set 10^{-4}. In this study MQ-RBF is used in the new meshless scheme MS as a basis function. For each data point (x_j, y_j), MQ-RBF is defined in the below equation.

$$\varphi_j(x,y) = \sqrt{c^2 + r_j^2} = \sqrt{c^2 + \left((x-x_j)^2 + (y-y_j)^2\right)}, \qquad (21)$$

where $r_j = \sqrt{(x-x_j)^2 + (y-y_j)^2}$.

Test 1: In this first test, the two algorithms GP and MS are compared for restoration performance of the in visual quality and PSNR values for real and artificial images "Butterfly", "Peppers", and SynImage2", respectively, that are displayed in Figures 1, 2, and 3. In the Figures, (a) and (b) shows true and noisy images while (c) and (d) represents images restored by the algorithms GP and MS. From these figures, it is clear that the restoration quality (visual quality and PSNR value) of proposed meshless scheme MS is better than GP. In GP, the image restoration is not bad but the issue is mainly due to the mesh-based scheme used in this algorithm. These obtained images are displayed in Figures 1(c), 2(c), and 3(c). In proposed scheme MS, the restoration results are better than that of GP regarding the image restoration (visual quality and increase in PSNR values) because of the meshless applications of MQ-RBF used in proposed scheme.

Furthermore, we can also see from Table 1 that the iterative numbers and the time of computation required for convergence of MS is less in comparison to GP which indicate the quick restoration because of the application of Kansa scheme MS over GP. The shape parameters c plays an important role for the smooth solution and quick convergence used in scheme MS. So the best selected range for the shape parameter values in this case 1 for all the three images is chosen as $1.79 \leq c \leq 1.84$.

Test 2: In this test, the real image '' SynImage2" is applied on the three techniques GP and MS to investigate homogeneity regarding loss or preservation.

To assess this reason a single line is chosen in the first picture and contrasted and similar lines of the recreated and noisy images that are shown in Figure 4. From displayed Figures 4(d), we can observe that resultant line reconstructed by MS is superior to GP which is given in Figures 4(c). Again, it can see from Figure 4 and Table 1, the performance (PSNR values, CUP times and number

of iterations required for convergence) of MS are better than that of GP.

Algorithm-1	Algorithm for meshless scheme MS
1.	**RBF:**
2.	
3.	Select $N = N_c$ number of n pixel data points.
4.	Calculate the value of β by using equation (12) through MQ-RBF.
5.	Find g according to the equation (14) by MQ-RBF using steps (1) and (2). Use equation (14) and calculate g by choosing MQ-RBF.
6.	**TV Regularization:**
7.	Select initial values for $\alpha_1, \alpha_2, c, \varepsilon, f,$ and dt.
8.	Choose n as Nc data centers pixel points $xc_1 \le xc_2 \le ..... \le xc_n,$ set n=0.
9.	Replace g in (15) as MQ-RBF. Here, $f^{(0)} = f$ is chosen.
10.	Then for $n = n+1,\ g^{n+1}$ by using Kansa method from equation (15), for each center data point
11.	xc_i, for $i = 1, 2, ..., n.$ $\dfrac{\left\|g^{n+1} - g^n\right\|}{\left\|g^n\right\|} \le \varepsilon = 10^{-5}$ (stopping condition), go to step (10). Otherwise again get to (7). End. Output result $g = g^{n+1}$.

Figure-1: Reconstructed images on Butterfly speckle noise; (a) Noiseless picture; (b) Noisy picture with $L = 0.1$; (c) Obtained picture using scheme GP $(\alpha_1 = 0.0001, \alpha_2 = 0.09)$ (d) Obtained picture using scheme MS $(\alpha_1 = 0.01, \alpha_2 = 0.02, c = 1.81)$

Figure-2: Recovered results on Peppers; (a) Noiseless picture; (b) Noisy picture $L = 0.1$; (c) Restored picture by method GP $(\alpha_1 = 0.0001, \alpha_2 = 0.07)$; (d) Restored picture by method MS $(\alpha_1 = 0.0001, \alpha_2 = 0.012, c = 1.82)$.

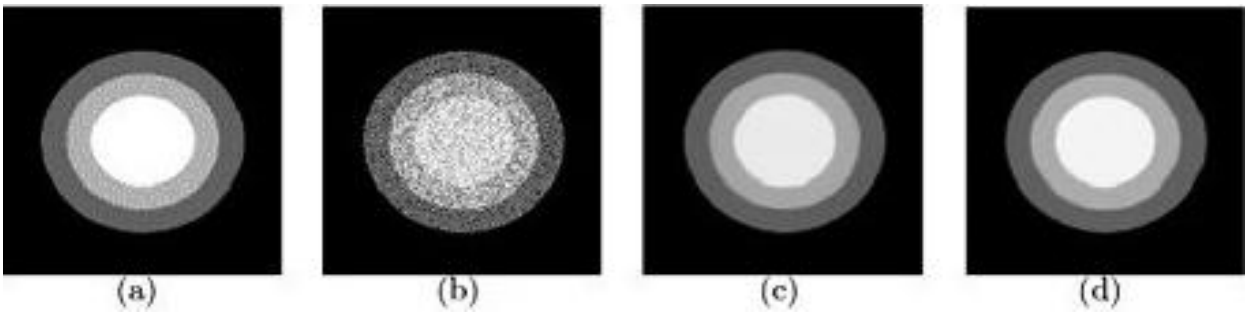

Figure-3: Recovered results on SynImage1; (a) Original image; (b) Noisy image $L = 0.1$; (c) Restored image by method GP $(\alpha_1 = 0.00011, \alpha_2 = 0.09)$; (d) Restored image by method MS $(\alpha_1 = 0.0001, \alpha_2 = 0.014, c = 1.83)$.

Table 1: Comparison of two schemes GP and MS.

Image	Size	GP scheme			MS scheme		
		PSNR	Iter	Time	PSNR	Iter	Time
Butterfly	300^2	23.21	422	190.21	24.59	239	101.23
Peppers	300^2	25.19	301	120.11	26.02	161	80.63
SynImage1	300^2	27.22	442	177.22	27.91	224	107.89
SynImgae2	300^2	24.71	411	164.82	25.22	202	95.27

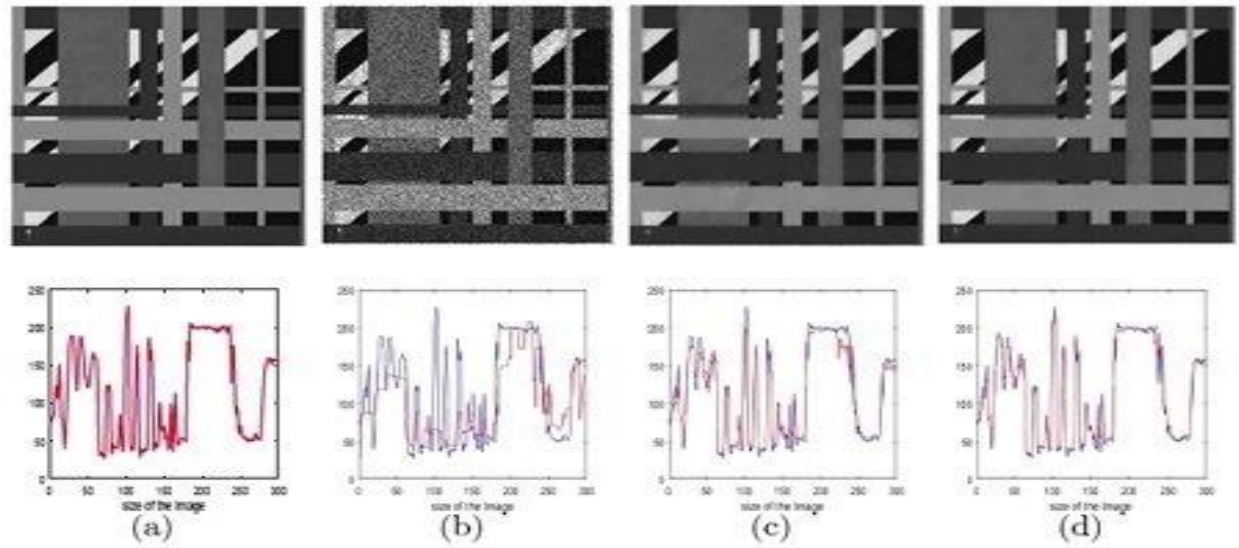

Figure-4: Recovered results on SynImage2; (a) Noiseless picture; (b) Noisy picture with $L = 0.1$; (c) Restored picture by method GP $(\alpha_1 = 0.0001, \alpha_2 = 0.08)$; (d) Restored picture by method MS $(\alpha_1 = 0.0001, \alpha_2 = 0.012, c = 1.83)$. It also shows Comparison of 107^{th} lines of Lena noiseless picture, the noisy picture with speckle noise, and restored images using algorithms GP and MS. (a) True image Line; (b) True and noisy lines; (c) Original and restored lines comparison using GP; (d) Original and reconstructed lines comparison using MS. The blue line shows the true picture line while the red line indicates the reconstructed picture line.

Analysis of the Shape Parameter: The purpose of this subsection is to investigate image restoration performance by the effect of shape parameter c used in our meshless method MS on artificial image "SynImage2". From the experimental results, we can observe that different shape parameter c values result in different

restoration performance (PSNR values) for the given image. These reconstructed images are displayed in Fig. 5 and Table 2. The parameters used in this case are $(\alpha_1 = 0.003, \alpha_2 = 0.07, c = 1.80)$

Table 2: Comparison of image restoration (PSNR) and shape parameter c values.

Image	Size	Best value c	PRNR	Increase in c	PSNR	Decrease in c	PSNR
SynImage3	300^2	1.80	26.19	1.89	25.87	1.72	25.68

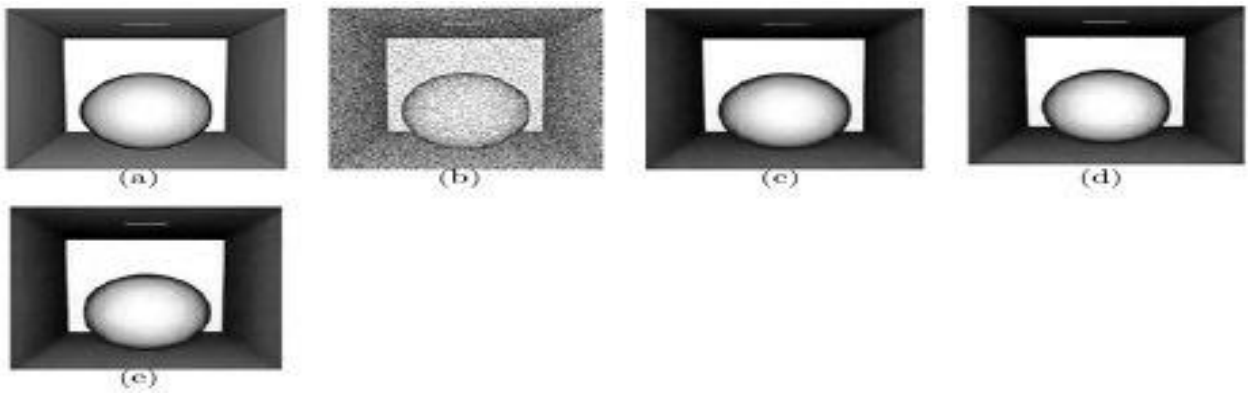

Figure-5: Experimental images on SynImage3 with Speckle noise; (a) Noiseless picture; (b) Noisy picture with $L = 0.07$; (c) Obtained picture using optimal value of $c = 1.80$; (d) Obtained picture using $c = 1.89$; (e) Obtained picture using $c = 1.72$.

Conclusion: In this study, a novel meshless scheme is introduced in which MQ-RBF is combined with a TV norm to solve the associated PDE with a model and to remove speckle noise from the model. This scheme is simple to implement and converge quickly. The results from the experimental results have shown that the proposed scheme is good in image restoration quality (PSNR value) and also have the faster convergence performance (CUP time and iterative numbers) compared with recent traditional TV-based scheme. The selection of shape parameters plays an essential role in the meshless scheme which can affect the restoration and convergence performance. A brief discussion for the the analysis of shape parameter has also given.

REFERENCES

Chen, W., Z.J. Fu and C.S. Chen (2014). *Recent advances in radial basis function collocation methods*. Heidelberg: Springer.

Chen, Y., S. Gottlieb, A. Heryudono and A. Narayan (2016). A reduced radial basis function method for partial differential equations on irregular domains. *Journal of Scientific Computing*, *66*(1), 67-90.

Dehghan, M., M. Abbaszadeh and A. Mohebbi (2015). A meshless technique based on the local radial basis functions collocation method for solving parabolic–parabolic Patlak–Keller–Segel chemotaxis model. *Engineering Analysis with Boundary Elements*, *56*, 129-144.

Jankowska, M.A., A. Karageorghis and C.S. Chen (2018). Kansa RBF method for nonlinear problems. *Boundary Elements and Other Mesh Reduction Methods*, 39.

Jiang, D.H., X. Tan, Y.Q. Liang and S. Fang (2015). A new nonlocal variational bi-regularized image restoration model via split Bregman method. *EURASIP Journal on Image and Video Processing*, *2015*(1), 15.

Khan, M.A., W. Chen, A. Ullah and Z. Fu (2017). A mesh-free algorithm for ROF model. *EURASIP Journal on Advances in Signal Processing*, *2017*(1), 53.

Li, F., C. Shen, J. Fan and C. Shen (2007). Image restoration combining a total variational filter and a fourth-order filter. *Journal of Visual Communication and Image Representation*, *18*(4), 322-330.

Singh, V. and S. Kumar (2017). Estimation of dispersion in an open channel from an elevated source using an upwind local meshless method. *International Journal of Computational Methods*, *14*(02), 1750009.

Shi, B., L. Huang and Z.F. Pang (2012). Fast algorithm for multiplicative noise removal. *Journal of Visual*

Communication and Image Representation, *23*(1), 126-133.

Sajavičius, S.N. (2013). Optimization, conditioning and accuracy of radial basis function method for partial differential equations with nonlocal boundary conditions—a case of two-dimensional Poisson equation. *Engineering Analysis with Boundary Elements*, *37*(4), 788-804.

Ullah, A., W. Chen and M.A. Khan (2016). A new variational approach for restoring images with multiplicative noise. *Computers & Mathematics with Applications*, *71*(10), 2034-2050.

Vertnik, R. and B. Šarler (2013). Local radial basis function collocation method along with explicit time stepping for hyperbolic partial differential equations. *Applied Numerical Mathematics*, *67*, 136-151.

Zhao, X.L., F. Wang and M.K. Ng (2014). A new convex optimization model for multiplicative noise and blur removal. *SIAM Journal on Imaging Sciences*, *7*(1), 456-475.